Research Square

Preprints are preliminary reports that have not undergone peer review.
They should not be considered conclusive, used to inform clinical practice,
or referenced by the media as validated information.

Integrative hdWGCNA and multi-model validation identify BAIAP2 as a shared neuronal hub for cognitive impairment acrossAlzheimer's disease, diabetic encephalopathy and brain aging

Husileng Hai
Tianjin University of Traditional Chinese Medicine
Yifang Luo
Tianjin University of Traditional Chinese Medicine
Jiale Ren
First Teaching Hospital of Tianjin University of Traditional Chinese Medicine
Weiwei Xue
Tianjin University of Traditional Chinese Medicine
Maojuan Guo
Tianjin University of Traditional Chinese Medicine
Zhen Yang
yzwygb@126.com
Tianjin University of Traditional Chinese Medicine

Research Article

Keywords: Alzheimer’s disease, diabetic encephalopathy, brain aging, single-cell sequencing, hdWGCNA, BAIAP2

Posted Date: November 3rd, 2026

DOI: https://doi.org/10.21203/rs.3.rs-11220228/v1

License: This work is licensed under a Creative Commons Attribution 4.0 International License.
Read Full License

Additional Declarations: No competing interests reported.

Abstract

Alzheimer's disease (AD), diabetic encephalopathy (DE), and brain aging converge on cognitive decline with overlapping synaptic damage, impaired neuronal plasticity, and hippocampal circuit dysfunction. However, whether these pathological states share a unified neuronal transcriptional architecture remains largely unexplored at single-cell resolution. Integrating single-cell transcriptomic datasets related to AD, DE, and brain aging from the GEO database with high-dimensional weighted gene co-expression network analysis, we identified a conserved neuronal module and hub genes shared across the pathological conditions, pinpointing BAIAP2/IRSp53 as the sole shared neuronal core gene. *In vivo*, mouse models of all three cognitive disorders exhibited significant spatial memory deficits and consistent downregulation of hippocampal BAIAP2 at both the mRNA and protein levels; immunofluorescence further confirmed a widespread reduction of BAIAP2 in the hippocampal CA1, CA3, and dentate gyrus regions. *In vitro*, amyloid-β, metabolic stress, and senescence-inducing stimuli each recapitulated BAIAP2 suppression in SH-SY5Y neurons. Collectively, we establish BAIAP2 as a critical synaptic scaffolding hub whose disruption represents a unified neuronal substrate linking neurodegeneration, metabolic brain injury, and brain aging. These findings identify BAIAP2 as a potential target for AD-spectrum therapeutic strategies against cognitive decline.

1. Introduction

With the accelerating global population aging, cognitive impairment has emerged as a major public health challenge threatening the health and quality of life of older adults[1, 2]. In 2015, there were approximately 47 million dementia patients worldwide, a number projected to rise to around 132 million by 2050[3, 4]. Cognitive disorders span a broad spectrum, including Alzheimer's disease (AD), vascular dementia, frontotemporal dementia, diabetic encephalopathy (DE), and age-associated cognitive decline[5]. Among these, AD, DE, and age-associated cognitive decline (brain aging) are representative. Despite their distinct primary etiologies, all three conditions ultimately perturb the same neuronal functional compartments—synaptic transmission, plasticity, and circuit integrity—raising the possibility that they may converge on shared molecular regulatory networks[6–8].

Current efforts to identify common mechanisms across AD, DE, and aging-related cognitive impairment have largely focused on individual pathways such as insulin signaling, oxidative stress, or neuroinflammation[9–11]. While informative, these pathway-centric approaches have yielded fragmented insights and have not systematically interrogated whether a unified transcriptional program operates within neurons themselves—the primary units of cognitive function. Moreover, conventional bulk-tissue analyses cannot distinguish whether transcriptional changes originate from neurons or from glial or vascular cells, nor can they resolve the cellular heterogeneity that may obscure neuron-specific core regulatory hubs. Recent advances in single-cell RNA sequencing (scRNA-seq) now make it possible to dissect transcriptional heterogeneity in complex brain tissue at cell-type resolution, while high-dimensional weighted gene co-expression network analysis (hdWGCNA) enables the construction of cell-type-specific co-expression networks and the identification of functional modules and hub genes

linked to pathological states[12]. Integrating these approaches provides a powerful strategy to uncover shared neuronal circuitry across distinct cognitive disorders.

Here, we integrated public single-cell transcriptomic datasets from AD, DE, and brain aging models, extracted neuronal populations, and performed neuron-specific hdWGCNA to identify conserved co-expression modules and hub genes across conditions. Intersection analysis pinpointed BAIAP2 as the sole shared neuronal core gene. We then validated its downregulation *in vivo* across three mouse models of cognitive impairment and in vitro under AD, DE, and aging-related stressors. Through this integrated strategy—from single-cell data mining to network biology to multi-model experimental confirmation—we demonstrate that BAIAP2 disruption represents a unified synaptic scaffolding mechanism bridging neurodegeneration, metabolic brain injury, and brain aging, positioning it as a molecular entry point for AD-spectrum therapeutic intervention against cognitive decline across etiologically distinct disorders.

BAIAP2 encodes the postsynaptic scaffolding protein IRSp53, which couples membrane curvature to Rho-family GTPase signaling and actin cytoskeletal remodeling, thereby regulating dendritic spine morphogenesis, postsynaptic density formation, and excitatory synaptic stability. BAIAP2/IRSp53 is enriched in hippocampal neurons and is functionally linked to NMDA receptor-mediated synaptic transmission and plasticity. Because the hippocampus—especially CA1, CA3, and dentate gyrus—is the principal substrate for spatial learning and memory and is consistently vulnerable in AD, DE, and brain aging, we focused on hippocampal BAIAP2 expression after identifying it as a shared neuronal hub gene by hdWGCNA. This rationale links the single-cell network finding to the Morris water maze phenotype and to the synaptic vulnerability shared by the three cognitive impairment models.

2. Materials and Methods

2.1. Single-cell transcriptomic data acquisition and preprocessing

Single-cell RNA sequencing datasets related to Alzheimer's disease (AD; GSE300079), diabetic encephalopathy (DE; GSE217665), and brain aging (GSE217560) were obtained from GEO. GSE300079 (AD-related) was derived from 6-month-old APOE4s2 inducible allelic-switch mice and included 10 whole-brain scRNA-seq samples: 4s2 Global Cre (n = 3), 4s2 Astrocyte Cre (n = 3), 4s2 no Cre (n = 1), E2-TR (n = 2), and E4-TR (n = 1); E4-TR and 4s2 no Cre were defined as APOE4 risk/AD-related groups, while E2-TR and 4s2 Global Cre were defined as APOE2 protective/switched groups. GSE217665 (DE) was derived from 16-week-old db/db type 2 diabetic and control mice and included two cerebral cortex scRNA-seq samples (diabetic n = 1, control n = 1); db/db mice were defined as the diabetes-associated cognitive decline model. GSE217560 (brain aging) was derived from C57BL/6J mice and included four brain scRNA-seq samples (CD 7m n = 1, HFD 7m n = 1, CD 12m n = 1, HFD 12m n = 1), with the original design reporting n = 3 mice per group; 18-month-old versus 9-month-old mice were defined as aging, and CD versus HFD was defined as metabolic stress. For the main aging analysis, CD brain samples were used, and HFD samples were used as a metabolic-stress sensitivity analysis. Because GSE217665

contained only one diabetic and one control cortex sample and GSE217560 provided one brain library per condition in the GEO sample list, the single-cell hdWGCNA analysis was considered discovery/exploratory, and the identified shared hub gene was validated in independent in vivo and in vitro experiments.

To ensure analytical uniformity, raw count matrices were processed and integrated using the Seurat (v5.3.0) and Harmony (v1.0) packages within the R environment (v4.3.0). Quality control (QC) thresholds were empirically optimized based on the distribution of sequencing metrics: cells with gene counts between 200 and 7,000, with unique molecular identifier (UMI) counts ≤ 30,000 and mitochondrial gene percentage ≤ 15% were retained. Potential doublets were identified and excluded using the Scrublet (v0.2.3) algorithm, applied separately to each sample prior to integration. After filtering low-abundance genes and low-quality cells, SCTransform was applied for data normalization and variance stabilization, and principal component analysis (PCA) was performed on highly variable genes. To mitigate technical confounders arising from inter-sample, inter-batch, and inter-dataset heterogeneity, the Harmony algorithm was applied to the PCA dimensionality reduction space to perform a soft-k means clustering correction.

Following batch-effect removal, a shared nearest neighbor (SNN) graph was constructed on the corrected Harmony embeddings by FindNeighbors and FindClusters for unsupervised clustering. Then, uniform manifold approximation and projection (UMAP) was performed for two-dimensional visualization. Differential expression analysis for each cluster was performed using the Wilcoxon rank-sum test to find marker genes and clusters were annotated based on the expression of canonical marker genes, cross-validated against the original dataset annotations.

2.2. Neuron-specific high-dimensional weighted gene co-expression network analysis (hdWGCNA)

To characterize neuronal co-expression network features shared across AD, DE, and brain aging, the hdWGCNA (v0.2.2) package was used to systematically analyze the annotated neuronal subsets. Given that technical and biological heterogeneity at the single-cell level can obscure true biological correlations, we aggregated single-cell expression profiles into “metacells” to generate a more robust correlation matrix. Specifically, using the MetacellsByGroups function, we aggregated cells with a minimum of 15 cells per metacell, grouping by the covariates of orig.ident, experimental condition, and neuronal subpopulation. This strategy effectively reduces data sparsity and balances the influence of sample-specific variations on co-expression estimation while preserving biological variance.

Following metacell construction, the optimal soft-thresholding power (β) for each dataset was determined using the TestSoftPowers across a range from 1 to 20. The optimal β was selected as the lowest value that achieved a scale-free topology model fit index (R^2) ≥ 0.85, while simultaneously ensuring robust mean connectivity to maintain the biological plausibility of the network topology. Based on the selected β, we employed the ConstructNetwork function to compute the signed topological overlap matrix (TOM), which minimizes spurious negative correlation and provides more biologically

interpretable adjacency measurements. Co-expression modules were subsequently identified via hierarchical clustering and the dynamic tree cut algorithm. Highly similar modules were merged to avoid redundancy using the mergeCutHeight parameter.

For each identified module, we calculated the module eigengenes via principal component analysis of the module expression matrix and computed intramodular connectivity to quantify the connectivity strength of individual genes within their respective modules. To link these networks to pathological phenotypes, module–trait correlation analysis was performed to identify neuronal modules significantly associated with disease status, and candidate hub genes were subsequently determined based on module membership and intramodular connectivity. Intersection analysis of hub genes from AD, DE, and brain aging-associated modules was conducted to pinpoint shared core neuronal genes.

2.3. Experimental animals and model establishment

All animal experimental protocols were approved by the Animal Ethics Committee of Tianjin University of Traditional Chinese Medicine (No.TCM-LAEC2024237R0915) and strictly conducted in accordance with the laboratory animal welfare and institutional ethical guidelines. Animals were housed under specific-pathogen-free (SPF) conditions with a temperature of 22 ± 2°C, relative humidity of 60 ± 5%, a 12 h light/dark cycle, and ad libitum access to food and water. All animals underwent a one-week acclimatization period prior to the initiation of experimental procedures.

For the brain aging model, 24-week-old male senescence-accelerated mouse prone 8 (SAMP8) mice were employed, with age -matched senescence-resistant control SAMR1 mice serving as the normal control group. Both strains were obtained from the Aged Mouse Breeding Base of the First Affiliated Hospital of Tianjin University of Traditional Chinese Medicine (SCXK(JIN)2019-0006). For the AD disease model, 24-week -old male APP/PS1 double transgenic mice were used, with non-transgenic C57BL/6J littermate mice as controls. For the DE model, 8-week-old male C57BL/6J mice were rendered diabetic via intraperitoneal (i.p.) injection of streptozotocin (STZ, Sigma-Aldrich, Cat# S0130) freshly dissolved in citrate buffer; control mice received an equal volume of citrate buffer vehicle. Diabetes induction was confirmed by measuring fasting blood glucose levels three days after the final STZ injection, and only mice with glucose levels ≥ 16.7 mM were included in the subsequent cognitive studies.

2.4. Morris water maze test

Spatial learning and memory were evaluated using the Morris water maze apparatus, consisting of a circular stainless-steel pool filled with water and maintained at 22 ± 1℃. A transparent circular escape platform (diameter: 10cm) was submerged 1.0 cm below the water surface in the center of the target quadrant. Distinctive extra-maze visual cues were affixed to the pool walls and remained constant through all trials.

The test comprised a place navigation phase and a spatial probe phase. During the place navigation phase, each mouse received one training trial per day over 5 consecutive days. At the start of each trial, the mouse was placed into the water facing the pool wall from one of four pseudo-randomly selected

start quadrants. The time taken to locate the hidden platform (escape latency) was recorded to assess its spatial learning ability. If a mouse failed to find the platform within the 60s cutoff, it was gently guided to the platform and allowed to remain there for 15s for spatial orientation. On day 6, the platform was removed, and each mouse was allowed to swim freely for 60s and spatial memory retention was assessed by measuring the time to first reach the original platform location, number of platform location crossings, time spent in the target quadrant, and swimming speed were recorded to assess spatial memory. All behavioral trajectories were automatically captured and analyzed by a video tracking system. Group allocation was blinded during both experimental operation and data analysis.

After behavioral evaluation, all mice were deeply anesthetized and euthanized. Brain tissues from three mice were fixed in 4% paraformaldehyde for immunofluorescence staining, while the hippocampi from the remaining mice were dissected out and stored at − 80°C for later use.

2.5. Immunofluorescence staining

Fixed brain tissues were sectioned into coronal frozen/paraffin sections to detect the expression and distribution of BAIAP2 protein in the hippocampus. Sections were rinsed with PBS, permeabilized with 0.25% Triton X-100 (Beyotime, Cat# ST1723) for 15 min at room temperature, and blocked with goat serum (Solarbio, Cat# SL038) to saturate non-specific binding sites. Subsequently, sections were incubated with rabbit anti-BAIAP2 polyclonal antibody (Proteintech, Cat# 11087-2-AP, RRID: AB_2063075; 1:200) overnight at 4°C in a humidified chamber. After three washes with PBS (5 min each), the sections were incubated with Alexa Fluor 488-conjugated goat anti-rabbit IgG (Thermo Fisher Scientific, Cat# A-11034, RRID: AB_2576217, diluted 1:500 in blocking buffer) in the dark. Nuclei were counterstained with DAPI contained in an antifade mounting medium (Servicebio, Cat# G1407-25ML), and the sections were then mounted with antifade mounting medium. As a negative control for antibody specificity, adjacent sections were processed identically but with the primary antibody omitted.

Whole-section panoramic images were acquired using a Pannoramic MIDI II digital slide scanner, with high-magnification cellular localization across all samples, the laser intensity, gain, and exposure time were strictly fixed for each fluorophore during acquisition. For quantitative analysis, anatomically matched regions of interest were delineated in the hippocampal CA1, CA3 and DG subregions. For each animal, three non-adjacent sections were analyzed, and three random fields of view were selected per subregion per section. The average MFI from these measurements was used for subsequent statistical comparison.

2.6. Cell culture and establishment *of in vitro* pathological injury models

SH-SY5Y cells (Procell, Cat# CL-0208) were cultured in DMEM/F12 medium (Gibco, Cat# 11330032) supplemented with 10% fetal bovine serum (FBS, ExCell Bio Cat# FSP500) and 1% penicillin-streptomycin (Gibco Cat# 15140122) at 37°C in a humidified atmosphere containing 5% CO_2. Cells in the logarithmic growth phase were used for experiments.

To recapitulate AD related amyloid-β neurotoxicity, DE associated metabolic stress, and aging-related injury, cells were exposed for 48h to the following agents, respectively: $A\beta_{25-35}$ (20 μg/mL, Sigma, Cat# A4559; prepared by pre-incubation at 37℃ for 7 days in sterile PBS to induce fibril formation), palmitic acid (PA, 10 μM, Sigma, Cat# P0500) and D-galactose (10 mM, Sigma, Cat# G0750). All treatments were performed in serum-containing complete medium without medium replacement during the 48 h incubation. After treatment, cells were harvested for subsequent analysis, and morphological changes were documented under an inverted phase- contrast microscope.

Cell viability was assessed using the CCK-8 assay (Life-iLab, Cat# AC11L054). Cells were seeded in 96-well plates at a density of 1.0×10^5 cells per well in 100 μL medium. After 48h treatment, CCK-8 working solution was added to each well according to the manufacturer's protocol.

2.7. RT-qPCR

RT-qPCR was used to detect the mRNA levels of BAIAP2 in mouse hippocampal tissue and SH-SY5Y cells. Total RNA was extracted using TRIzol Universal reagent (TIANGEN, Cat# DP424), and its purity was assessed by the A260/A280 ratio (1.8–2.1). Equal amounts of RNA were reverse-transcribed into cDNA using the FastKing RT Kit (TIANGEN, Cat# KR116) according to the manufacturer's instructions. RT-qPCR was performed using SuperReal PreMix Plus (SYBR Green) (TIANGEN, Cat# FP205), with the following thermal profile: 95°C for 30 s, followed by 40 cycles of 95°C for 5 s and 60°C for 30 s. Gapdh was used as the internal reference for mouse samples and GAPDH for human cells.

2.8. Western blot analysis

Hippocampal tissue and SH-SY5Y cell samples were lysed in RIPA buffer (Servicebio, Cat# G2002-100ML), and supernatants were collected after low-temperature centrifugation. Protein concentrations were quantified using the BCA assay (Beyotime, Cat# P0009). Equal amounts of protein (10 μg per lane) were separated by SDS-PAGE, wet-transferred to PVDF membranes (Thermo Fisher Scientific, Cat# 88518), and blocked with rapid blocking solution. Membranes were incubated overnight at 4°C with primary antibodies against BAIAP2 antibody (Proteintech, Cat# 11087-2-AP, RRID: AB_2063075, 1:1000) and β-actin antibody (Proteintech, Cat# 66009-1-Ig, RRID: AB_2687938, 1:10000). After three washes with TBST, the membranes were incubated with HRP-conjugated goat anti-rabbit IgG (Proteintech, Cat# SA00001-2, RRID: AB_2722564,1:10000) and goat anti-mouse IgG (Proteintech, Cat# RGAM001, RRID: AB_3068333,1:10000) for 2h at room temperature. Immunoreactive bands were visualized using ECL chemiluminescence (Beijing Zoman Biotechnology Co., Ltd., Cat# ZD310-10) and captured with a chemiluminescence imaging system. Densitometric analysis was performed using ImageJ software and relative BAIAP2 protein expression was normalized to β-actin levels. All experiments were repeated in three independent biological replicates.

2.9. Statistical analysis

Bioinformatic data processing and differential expression analyses were performed in R (v4.3.0) and visualized with GraphPad Prism (v9.0). Comparisons between two groups were performed using an

unpaired two-tailed Student's t-test; while multiple-group comparisons were evaluated by one-way ANOVA followed by Tukey's multiple comparison test. For high-dimensional single-cell transcriptomic data, multiple hypothesis testing was corrected using Benjamini–Hochberg method, with an adjusted P-value or FDR < 0.05 considered statistically significant. Quantitative data are presented as mean ± standard deviation (SD) and all sample sizes (n) along with *P*-values or FDRs are detailed in the figure legends.

3. Results

3.1. Single-cell integrative analysis defines the brain cellular landscape across AD, DE and aging

To characterize the cellular landscape associated with Alzheimer's disease (AD), diabetic encephalopathy (DE), and brain aging, three single-cell RNA sequencing datasets were analyzed in parallel. Following quality control, normalization, dimensionality reduction, and unsupervised clustering, UMAP visualization resolved multiple transcriptionally distinct cell clusters within each dataset (Fig. 1A-C).

We subsequently assigned biological identities to these clusters based on the expression of canonical cell-type marker genes. The annotated UMAPs revealed diverse neuronal, glial, vascular, immune, and other brain-associated cell populations across the three datasets (Fig. 1D-F). Major populations included neurons, astrocytes, oligodendrocytes, microglia, endothelial cells, pericytes, macrophages, fibroblasts, and choroid plexus epithelial cells, together with several dataset-specific populations such as oligodendrocyte precursor cells, neuroblasts, neural progenitor/radial glial cells, ependymal cells, smooth muscle cells, T cells, and neutrophils.

The validity of these annotations was further supported by the expression patterns of representative lineage-specific markers (Fig. 1G-I). For example, neuronal populations were characterized by neuronal markers including Rbfox3, Map2, Syt1, and Snap25; astrocytes expressed Gfap, Aldh1l1, and Aqp4; microglia were enriched for Tmem119, P2ry12, Cx3cr1, C1qa, and C1qb; and oligodendrocytes showed prominent expression of Mbp, Plp1, Mog, and Opalin. Vascular populations were distinguished by endothelial markers such as Pecam1 and Cldn5 and pericyte-associated markers including Pdgfrb, Rgs5, Vtn, and Abcc9. Additional populations were similarly supported by their characteristic marker expression profiles, including Dcx in neuroblasts, Col1a1 or Dcn in fibroblasts, Mrc1 and Cd163 in macrophages, and Ttr and Folr1 in choroid plexus epithelial cells.Together, the concordance between unsupervised clustering, cell-type annotation, and canonical marker expression supported the robustness of the cellular assignments across the three datasets. These analyses enabled the reliable identification and extraction of neuronal populations for subsequent neuron-specific co-expression network analysis.

3.2. hdWGCNA identifies BAIAP2 as a shared hub gene in neuronal modules across AD, DE and aging

To identify conserved neuronal transcriptional programs associated with AD, DE, and brain aging, neuron-specific high-dimensional weighted gene co-expression network analysis (hdWGCNA) was performed independently in the three single-cell datasets. Based on neuronal subtype characterization, representative neuronal populations were selected for subsequent co-expression network construction (Fig. 2A-C). Prior to module detection, the optimal soft-thresholding powers were determined for each dataset to establish scale-free network topology. The selected parameters achieved high scale-free topology fitting while maintaining appropriate network connectivity, supporting the reliability of the constructed neuronal co-expression networks.

Hierarchical clustering of neuronal gene expression profiles subsequently identified distinct co-expression modules within each pathological condition (Fig. 2D-F). Module eigengene analysis revealed specific neuronal modules preferentially associated with each pathological state, including an AD-associated module enriched in Neurons3, a DE-associated module enriched in Neurons7, and an aging-associated module enriched in Neurons30.

To identify shared molecular regulators underlying cognitive impairment across distinct pathological conditions, hub genes from the disease-associated neuronal modules were extracted and compared. Intersection analysis revealed BAIAP2 as the only common hub gene shared among AD, DE, and aging-associated neuronal modules (Fig. 2G). These findings indicate that diverse pathological insults converge on a conserved neuronal transcriptional network centered on BAIAP2.

3.3. Decreased BAIAP2 expression in the hippocampus of model mice confirmed by behavioral and molecular assays

To determine whether BAIAP2, identified as a shared neuronal hub gene from single-cell transcriptomic and hdWGCNA analyses, is dysregulated *in vivo*, we examined its hippocampal expression and the associated cognitive phenotypes in model mice.

Spatial learning and memory were first assessed using the Morris water maze. During the place navigation phase, escape latencies of control mice declined progressively across training days, whereas model mice consistently took longer to locate the hidden platform. At the end of training, model groups showed significantly longer latencies than their respective controls ($P < 0.01$, Fig. 3A). In the subsequent probe trial, model groups crossed the former platform location significantly fewer times ($P < 0.01$, Fig. 3B) and took significantly longer to first reach the platform location ($P < 0.01$, Fig. 3C) compared with controls. These results indicate that the model mice developed robust learning and memory impairment.

The expression of BAIAP2 in the hippocampus of model mice was assessed. RT-qPCR revealed a significant reduction in BAIAP2 mRNA levels in model groups compared with controls ($P < 0.01$, Fig. 3F). Western blotting further demonstrated a corresponding decrease in BAIAP2 protein abundance (Fig. 3D), and quantification confirmed a significant reduction compared with controls ($P < 0.01$, Fig. 3E).

Collectively, BAIAP2 was downregulated at both transcriptional and translational levels in the hippocampus of cognitively impaired model mice.

3.4. Immunofluorescence reveals downregulation of BAIAP2 in hippocampus of model mice

To examine the regional distribution of BAIAP2 in the hippocampus, immunofluorescence staining was performed on brain sections from control and model mice, with DAPI nuclear counterstaining. The results showed that BAIAP2-positive signals were distributed across hippocampal CA1, CA3, and DG regions, predominantly localized around DAPI-positive nuclei and in the neuropil-like areas of the hippocampus (Fig. 4A). Quantitative analysis of mean fluorescence intensity showed that BAIAP2 levels were significantly lower in model mice than in controls in CA1 ($P < 0.01$, Fig. 4B), CA3 ($P < 0.01$, Fig. 4C) and DG ($P < 0.01$, Fig. 4D). These results indicate a consistent downregulation of BAIAP2 across these hippocampal subregions in AD, DE and aging model mice.

3.5. BAIAP2 is downregulated in SH-SY5Y cell models of neuronal injury

To further verify BAIAP2 expression under conditions mimicking the three disease context, SH-SY5Y cells were treated with $A\beta_{25\text{-}35}$, palmitic acid (PA), or D-galactose to model AD-related amyloid toxicity, DE-related lipotoxicity/metabolic stress, and aging-associated cellular damage, respectively. The concentrations of PA and D-galactose were selected based on CCK-8 viability assays, and finally 10 μmol/L PA and 10 mmol/L D-galactose were selected for not affecting cell viability (Fig. 5A, 5B). The $A\beta_{25-35}$ concentration was adopted from a previous report (20 μg/mL)[13].

Following the respective treatments, BAIAP2 expression was quantified by RT-qPCR and western blotting. Western blotting revealed decreased BAIAP2 protein abundance in all three treatment groups compared with the normal control group (Fig. 5C), and densitometric analysis confirmed a significant reduction ($P < 0.01$, Fig. 5D). Consistently, all three treatment groups showed significantly reduced BAIAP2 mRNA levels compared with untreated control cells ($P < 0.01$, Fig. 5F). These results indicate that BAIAP2 is consistently downregulated at both transcript and protein levels across all three in vitro injury models.

4. Discussion

Alzheimer's disease (AD), diabetic encephalopathy (DE), and brain aging are three clinically distinct conditions that nevertheless share a final common pathway of hippocampal-dependent cognitive decline. AD is pathologically characterized by extracellular amyloid-β plaques, intracellular neurofibrillary tangles composed of hyperphosphorylated tau, and progressive loss of synapses and neurons, particularly within the entorhinal–hippocampal circuit[14–16]. DE, a chronic complication of diabetes mellitus, arises from sustained hyperglycemia, insulin resistance, advanced glycation end-product

accumulation, and low-grade neuroinflammation, which together impair synaptic plasticity and promote neuronal injury in the hippocampus[17–19]. Brain aging, even in the absence of overt neurodegenerative disease, is accompanied by mitochondrial dysfunction, oxidative stress, altered proteostasis, and reductions in synaptic protein expression and dendritic spine density[20–22]. Despite their different primary triggers, all three conditions converge on synaptic failure—especially in hippocampal CA1, CA3, and dentate gyrus regions—suggesting that neurons may activate or suppress a common transcriptional program under diverse pathological stresses[23, 24]. This convergence provides the rationale for the present study to search for shared neuronal hub genes across AD, DE, and aging-related cognitive impairment at single-cell resolution[25, 26].

In this study, single-cell transcriptomic profiling combined with neuron-specific weighted gene co-expression network analysis was performed to investigate whether distinct etiologies of cognitive impairment—AD, DE, and brain aging models—share convergent transcriptional remodeling in neurons. We identified BAIAP2 as the only shared neuronal hub gene across these three cognitive impairment-associated conditions and validated its consistently downregulated expression at the spatial tissue level, as well as both the transcript and protein levels in both *in vivo* and *in vitro* models. These findings position BAIAP2 as a potential common nodal point linking diverse pathological insults to neuronal dysfunction.

Previous studies have largely focused on pathway—specific mediators—such as amyloid-β deposition, tau hyperphosphorylation, insulin resistance, or oxidative stress—in isolation, which has limited our understanding of why such distinct upstream triggers ultimately produce overlapping cognitive phenotypes[27]. By applying high-dimensional weighted gene co-expression network analysis (hdWGCNA) at single-cell resolution, we effectively minimized compositional confounding from non-neuronal cell types and revealed that neurons under these three pathological states undergo strikingly similar modular restructuring. This observation shifts the conceptual framework from shared terminal phenotypes to shared systems-level transcriptional network reconfiguration, suggesting that synaptic dysfunction in these conditions may represent a common effector pathway rather than a mere epiphenomenon of individual disease cascades.

BAIAP2 encodes a postsynaptic scaffolding protein that couples membrane curvature through its N-terminal IMD/I-BAR domain while simultaneously integrating Rho family small GTPase signals via its C-terminal SH3 domain[28–30], thereby coordinating actin cytoskeleton dynamics with spine morphogenesis[31]. This function. nthe primary structural basis for excitatory synaptic transmission[32], their morphology and density directly determine synaptic transmission efficacy and neural circuit plasticity. Thus, BAIAP2 serves as a critical structural bridge between molecular signaling and neural circuit function[33]. Our study revealed that BAIAP2 downregulation exhibits high spatial consistency across the hippocampal CA1, CA3, and DG regions, implying a broad disruption of the trisynaptic circuit rather than a subregion-restricted effect. Importantly, this downregulation was consistently observed not only in AD-related pathological conditions but also under metabolic stress and aging-like stimulus. Furthermore, the fact that BAIAP2 downregulation was recapitulated *in vitro* by $A\beta_{25-35}$, palmitic acid, and

D-galactose—each representing a distinct primary insult—reinforces the idea that BAIAP2 functions as a general stress-responsive node, rather than a disease-specific marker.

Collectively, these findings support a convergent neuronal vulnerability model: disparate upstream drivers (proteotoxicity, metabolic stress, and chronological aging) may funnel into a common downstream axis centered on BAIAP2-mediated synaptic actin cytoskeleton regulation. Disruption of this axis, we propose, leads to spine destabilization, reduced synaptic efficacy, and ultimately, the shared cognitive phenotypes observed across these diseases. While this model is conceptually parsimonious and biologically grounded, it remains correlational at this stage and requires direct causal testing.

Nevertheless, this study has several limitations. The current conclusions are derived from correlational expression data, the sufficiency and necessity of BAIAP2 in driving the observed cognitive deficits have not been established. Additionally, the upstream transcriptional or epigenetic regulators responsible for BAIAP2 downregulation under these distinct stressors remain unexplored, and it remains an open question whether they converge on a shared promoter element or microRNA network.

In conclusion, this study reframes the molecular pathology of diverse cognitive disorders by shifting from a single-etiology perspective to a shared structural susceptibility of neurons. BAIAP2 emerges as a synaptic scaffolding hub whose consistent downregulation may represent a common neuronal substrate for cognitive decline. This insight not only provides a unified framework for understanding disease convergence but also highlights the modulation of synaptic cytoskeletal dynamics as a promising arena for developing broad-spectrum therapeutic strategies against cognitive dysfunction of heterogeneous origins.

CRediT authorship contribution statement

Husileng Hai: Writing – original draft, Formal analysis, Visualization, Investigation. **Yifang Luo**: Writing – review & editing, Methodology, Formal analysis. **Jiale Ren**: Writing – original draft, Methodology, Data curation, Validation. **Weiwei Xue**: Writing – review & editing, Methodology, Formal analysis. **Maojuan Guo**: Writing – review & editing, Supervision, Resources. **Zhen Yang**: Writing – review & editing, Supervision, Project administration, Funding acquisition.

Declarations

Declaration of Competing Interest

The authors declare that they have no known competing financial interests or personal relationships that could have appeared to influence the work reported in this paper.

Ethics approval and consent to participate

All animal experimental protocols were approved by the Animal Ethics Committee of Tianjin University of Traditional Chinese Medicine (Approval No.: TCM-LAEC2024237R0915).

Consent for publication

This study did not contain any person's data in any form (including details, images, or videos). Therefore, additional consent for publication beyond the informed consent obtained from all participants (as described in the "Methods" section) is not required.

Funding

This work was supported by the National Natural Science Foundation of China (No. 82304896) and Tianjin Municipal Health Commission—Research Projects in Key Areas of Traditional Chinese Medicine (No. 2024010).

Author Contribution

H.H.: Writing – original draft, Formal analysis, Visualization, Investigation. Y.L.: Writing – review & editing, Methodology, Formal analysis. J.R.: Writing – original draft, Methodology, Data curation, Validation. W.X.: Writing – review & editing, Methodology, Formal analysis. M.G.: Writing – review & editing, Supervision, Resources. Z.Y.: Writing – review & editing, Supervision, Project administration, Funding acquisition. All authors reviewed the manuscript.

Acknowledgement

The authors acknowledge the collaborative efforts and contributions of every author involved in this project. We extend our sincere appreciation to Zhen Yang, our corresponding author, for her expert leadership, critical review, and steadfast support during the research and manuscript preparation.

Availability of data and materials

All data generated and analyzed in this study are included in this article. Data will be made available on request.

References

1. Wu X, Tang Y, He Y, Wang Q, Wang Y, Qin X (2024) Prevalence of cognitive impairment and its related factors among Chinese older adults: an analysis based on the 2018 CHARLS data. Front Public Health 12:1500172. https://doi.org/10.3389/fpubh.2024.1500172

2. Kang M, Lee I, Hong H, Kim J, Kang H (2021) Predictors of changes in cognitive function in older Korean adults: the 2006–2018 Korean Longitudinal Study of Aging. Int J Environ Res Public Health 18:6345. https://doi.org/10.3390/ijerph18126345
3. Zhang R, Liu S, Mousavi SM (2024) Cognitive dysfunction and exercise: from epigenetic to genetic molecular mechanisms. Mol Neurobiol 61:6279–6299. https://doi.org/10.1007/s12035-024-03970-7
4. Prickaerts J, Kerckhoffs J, Possemis N, van Overveld W, Verbeek F, Grooters T et al (2024) Roflumilast and cognition enhancement: a translational perspective. Biomed Pharmacother 181:117707. https://doi.org/10.1016/j.biopha.2024.117707
5. Weidung B, Lövheim H, Littbrand H, Wahlin J, Olofsson B, Gustafson Y (2023) Temporal dementia and cognitive impairment trends in the very old in the 21st century. J Alzheimers Dis 93:61–74. https://doi.org/10.3233/JAD-220915
6. Tzioras M, McGeachan RI, Durrant CS, Spires-Jones TL (2023) Synaptic degeneration in Alzheimer disease. Nat Rev Neurol 19:19–38. https://doi.org/10.1038/s41582-022-00749-z
7. Ahlawat A, Walia V, Garg M (2025) Brain insulin resistance mediated cognitive impairment and neurodegeneration: type-3 diabetes or Alzheimer's disease. Acta Neurol Belg 125:941–969. https://doi.org/10.1007/s13760-024-02706-7
8. Apaijai N, Attachaipanich T, Maneechote C, Pintana H, Thonusin C, Chunchai T (2025) Sodium-glucose cotransporter 2 inhibitor partially improves brain mitochondrial function, but does not mitigate cognitive impairment in rats with myocardial infarction. Biochim Biophys Acta Mol Basis Dis 1871:167809. https://doi.org/10.1016/j.bbadis.2025.167809
9. Lanzillotta S, Rolfi LR, Zulli B et al (2026) Metabolic breakdown: linking insulin resistance and mitochondrial dysfunction to neurodegeneration in Alzheimer's disease. Neural Regen Res 21:2227–2237. https://doi.org/10.4103/NRR.NRR-D-25-00144
10. Lanzillotta S, Rolfi LR, Zulli B, Barone E (2023) Chemogenetic emulation of intraneuronal oxidative stress affects synaptic plasticity. Redox Biol 60:102604. https://doi.org/10.1016/j.redox.2023.102604
11. Wu XM, Shi CN, Liu K, Hu XY, He QL, Yao H (2025) Decreased excitatory and increased inhibitory transmission in the hippocampal CA1 drive neuroinflammation-induced cognitive impairments in mice. Brain Behav Immun 128:416–428. https://doi.org/10.1016/j.bbi.2025.04.027
12. Fastrès A, Pirottin D, Fievez L, Marichal T, Desmet CJ, Bureau F (2020) Characterization of the bronchoalveolar lavage fluid by single cell gene expression analysis in healthy dogs: a promising technique. Front Immunol 11:1707. https://doi.org/10.3389/fimmu.2020.01707
13. Ren J, Xiang B, Song L, René DJ, Luo Y, Wen G (2024) Kaixinsan regulates neuronal mitochondrial homeostasis to improve the cognitive function of Alzheimer's disease by activating CaMKKβ-AMPK-PGC-1α signaling axis. Phytomedicine 135:156170. https://doi.org/10.1016/j.phymed.2024.156170
14. Rodriguez-Jimenez FJ, Ureña-Peralta J, Jendelova P, Erceg S (2023) Alzheimer's disease and synapse loss: what can we learn from induced pluripotent stem cells? J Adv Res 54:105–118.

https://doi.org/10.1016/j.jare.2023.01.006

15. Fan X, Wang H, Ping J, Li M, Gu J, Qian W (2025) Synaptic scaffold protein PSD-95: a therapeutic target for Alzheimer's disease. Biochem Pharmacol 242:117401. https://doi.org/10.1016/j.bcp.2025.117401
16. Alldred MJ, Ibrahim KW, Pidikiti H, Lee SH, Heguy A, Chiosis G et al (2025) Profiling hippocampal neuronal populations reveals unique gene expression mosaics reflective of connectivity-based degeneration in the Ts65Dn mouse model of Down syndrome and Alzheimer's disease. Front Mol Neurosci 18:1546375. https://doi.org/10.3389/fnmol.2025.1546375
17. Videtta G, Sasia C, Galeotti N (2025) High rosmarinic acid content Melissa officinalis L. phytocomplex modulates microglia neuroinflammation induced by high glucose. Antioxid (Basel) 14:161. https://doi.org/10.3390/antiox14020161
18. Fang XX, Xu FF, Liu Z, Cao BB, Qiu YH, Peng YP (2022) Interleukin 17A deficiency alleviates neuroinflammation and cognitive impairment in an experimental model of diabetic encephalopathy. Neural Regen Res 17:2771–2777. https://doi.org/10.4103/1673-5374.339490
19. Hua MY, Huang S, Zhuang ZY, Han XL, Liu XJ, Liang ZH (2026) Microglial NLRP3-dependent pyroptosis promotes cognitive dysfunction of diabetic encephalopathy by inhibiting adult hippocampal neurogenesis through the release of IL-1β. Acta Pharmacol Sin 47:2049–2064. https://doi.org/10.1038/s41401-026-01774-0
20. Cicali KA, Tapia-Rojas C (2024) Synaptic mitochondria: a crucial factor in the aged hippocampus. Ageing Res Rev 101:102524. https://doi.org/10.1016/j.arr.2024.102524
21. Cicali KA, Torres AK, Tapia-Rojas C (2026) Synaptic mitochondria in aging and neurodegenerative diseases: functional decline and vulnerability. Neural Regen Res 21:2145–2152. https://doi.org/10.4103/NRR.NRR-D-24-01571
22. Krivinko JM, Fan P, Sui Z, Happe C, Hensler C, Gilardi J (2025) Age-related loss of large dendritic spines in the precuneus is statistically mediated by proteins which are predicted targets of existing drugs. Mol Psychiatry 30:2059–2067. https://doi.org/10.1038/s41380-024-02817-w
23. Bouwman MMA, Frigerio I, Graaf YG, van de Berg WDJ, Jonkman LE (2026) Distinct regional patterns of synaptic vulnerability across hippocampal and parahippocampal subregions in Alzheimer's disease. Brain Pathol 36:e70081. https://doi.org/10.1111/bpa.70081
24. Castro CCM, Silva SP, Rabelo LN, Queiroz JPG, Campos LD, Silva LC (2022) Age, education years, and biochemical factors are associated with selective neuronal changes in the elderly hippocampus. Cells 11:4033. https://doi.org/10.3390/cells11244033
25. Jin W, Pei J, Roy JR, Jayaraman S, Ahalliya RM, Kanniappan GV (2024) Comprehensive review on single-cell RNA sequencing: a new frontier in Alzheimer's disease research. Ageing Res Rev 100:102454. https://doi.org/10.1016/j.arr.2024.102454
26. Mathys H, Boix CA, Akay LA, Xia Z, Davila-Velderrain J, Ng AP (2024) Single-cell multiregion dissection of Alzheimer's disease. Nature 632:858–868. https://doi.org/10.1038/s41586-024-07606-7

27. Ju Y, Tam KY (2022) Pathological mechanisms and therapeutic strategies for Alzheimer's disease. Neural Regen Res 17:543–549. https://doi.org/10.4103/1673-5374.320970
28. Lee SE, Kim JA, Chang S (2018) nArgBP2-SAPAP-SHANK, the core postsynaptic triad associated with psychiatric disorders. Exp Mol Med 50:1–9. https://doi.org/10.1038/s12276-017-0018-5
29. Kast DJ, Dominguez R (2019) Mechanism of IRSp53 inhibition by 14-3-3. Nat Commun 10:483. https://doi.org/10.1038/s41467-019-08317-8
30. Zhang G, Lu Y, Xie L, Begemann A, Papuc SM, Zweier M (2026) De novo missense variants in BAIAP2 are associated with developmental and epileptic encephalopathies. Epilepsia 67:480–498. https://doi.org/10.1111/epi.18661
31. Feng Z, Lee S, Jia B, Jian T, Kim E, Zhang M (2022) IRSp53 promotes postsynaptic density formation and actin filament bundling. J Cell Biol 221:e202105035. https://doi.org/10.1083/jcb.202105035
32. Khanal P, Hotulainen P (2021) Dendritic spine initiation in brain development, learning and diseases and impact of BAR-domain proteins. Cells 10:2392. https://doi.org/10.3390/cells10092392
33. Noh YW, Yook C, Kang J, Lee S, Kim Y, Yang E (2022) Adult re-expression of IRSp53 rescues NMDA receptor function and social behavior in IRSp53-mutant mice. Commun Biol 5:838. https://doi.org/10.1038/s42003-022-03813-y

Figures

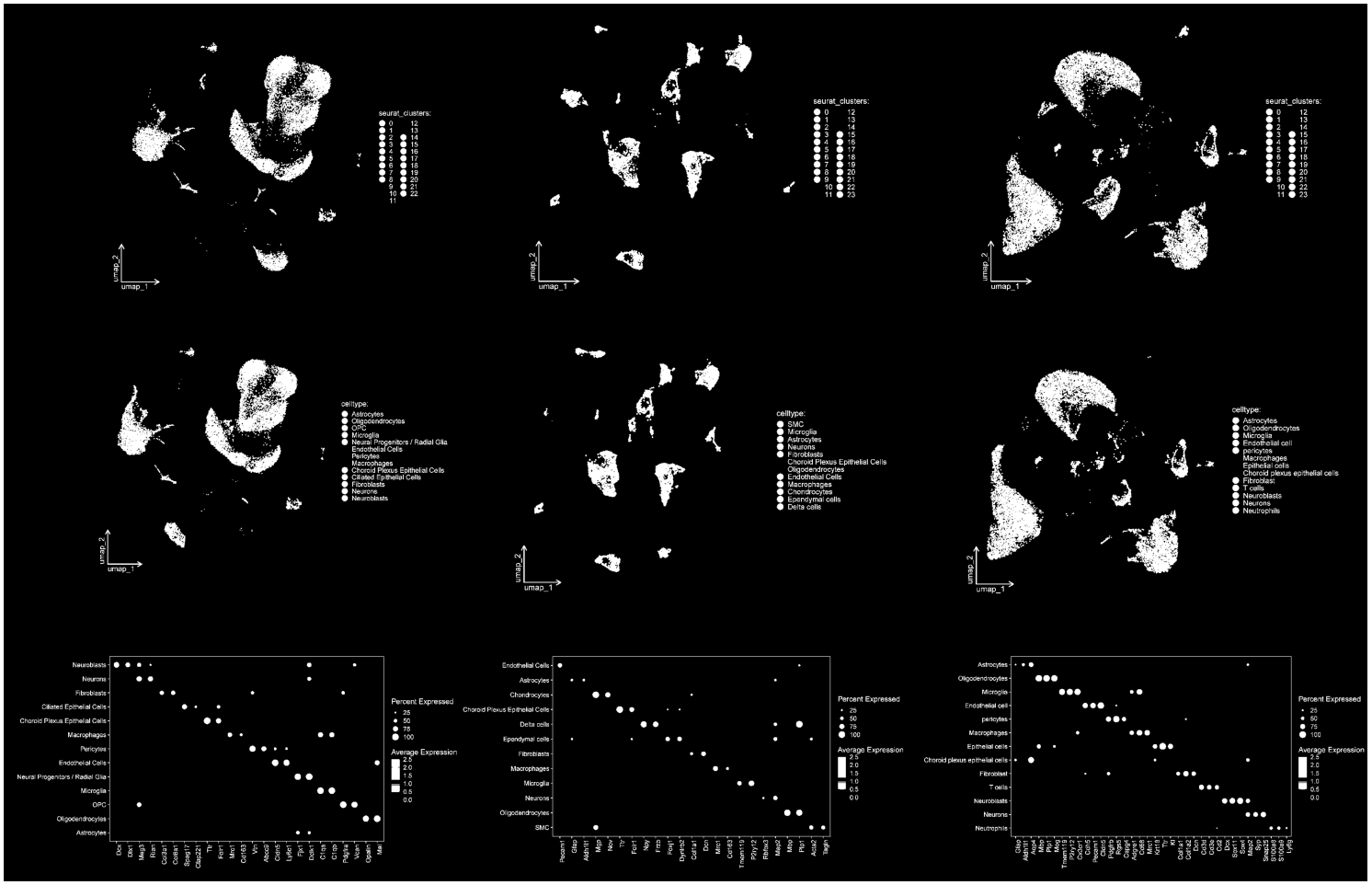

Figure 1

Single-cell transcriptomic profiling delineates the cellular landscape across Alzheimer's disease, diabetic encephalopathy, and brain aging. (A-C) UMAP visualization of unsupervised cell clusters in the Alzheimer's disease (AD), diabetic encephalopathy (DE), and brain aging datasets, respectively, following quality control, normalization, and batch-effect correction. Cells are colored according to unsupervised cluster identity. (D-F) UMAP visualization of the corresponding datasets after cell-type annotation based on canonical lineage-specific marker genes. Distinct neuronal, glial, vascular, immune, and other brain-associated cell populations were identified in each dataset. (G-I) Dot plots showing the expression patterns of representative canonical marker genes across the annotated cell populations in the AD, DE, and brain aging datasets, respectively. Dot size represents the percentage of cells expressing the indicated gene, whereas color intensity represents the scaled average expression level.

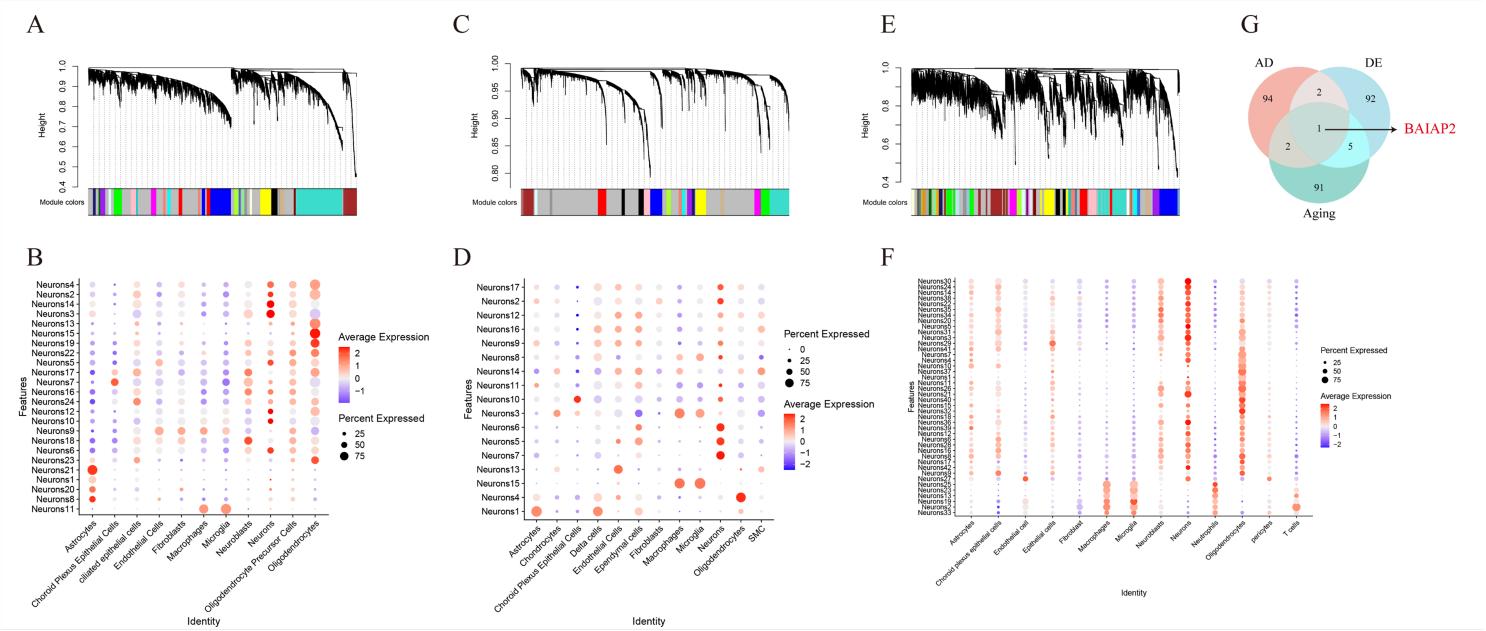

Figure 2

Neuron-specific hdWGCNA identifies BAIAP2 as a shared hub gene across Alzheimer's disease, diabetic encephalopathy, and brain aging. (A, C, E) Hierarchical clustering dendrograms generated by neuron-specific high-dimensional weighted gene co-expression network analysis (hdWGCNA) for the AD, DE, and brain aging datasets, respectively. Genes with similar co-expression patterns were grouped into modules, with module assignments indicated by different colors beneath each dendrogram. (B, D, F) Dot plots showing the expression patterns of the identified co-expression modules across annotated brain cell populations in the corresponding AD, DE, and brain aging datasets. These analyses highlighted the neuron-enriched modules Neurons3, Neurons7, and Neurons30 in the AD, DE, and brain aging datasets, respectively. Dot size indicates the percentage of cells contributing to the indicated feature, and color represents the scaled average expression level. (G) Venn diagram showing the intersection of candidate hub genes derived from the selected neuronal modules in the three datasets. BAIAP2 was the only hub gene shared among AD, DE, and brain aging.

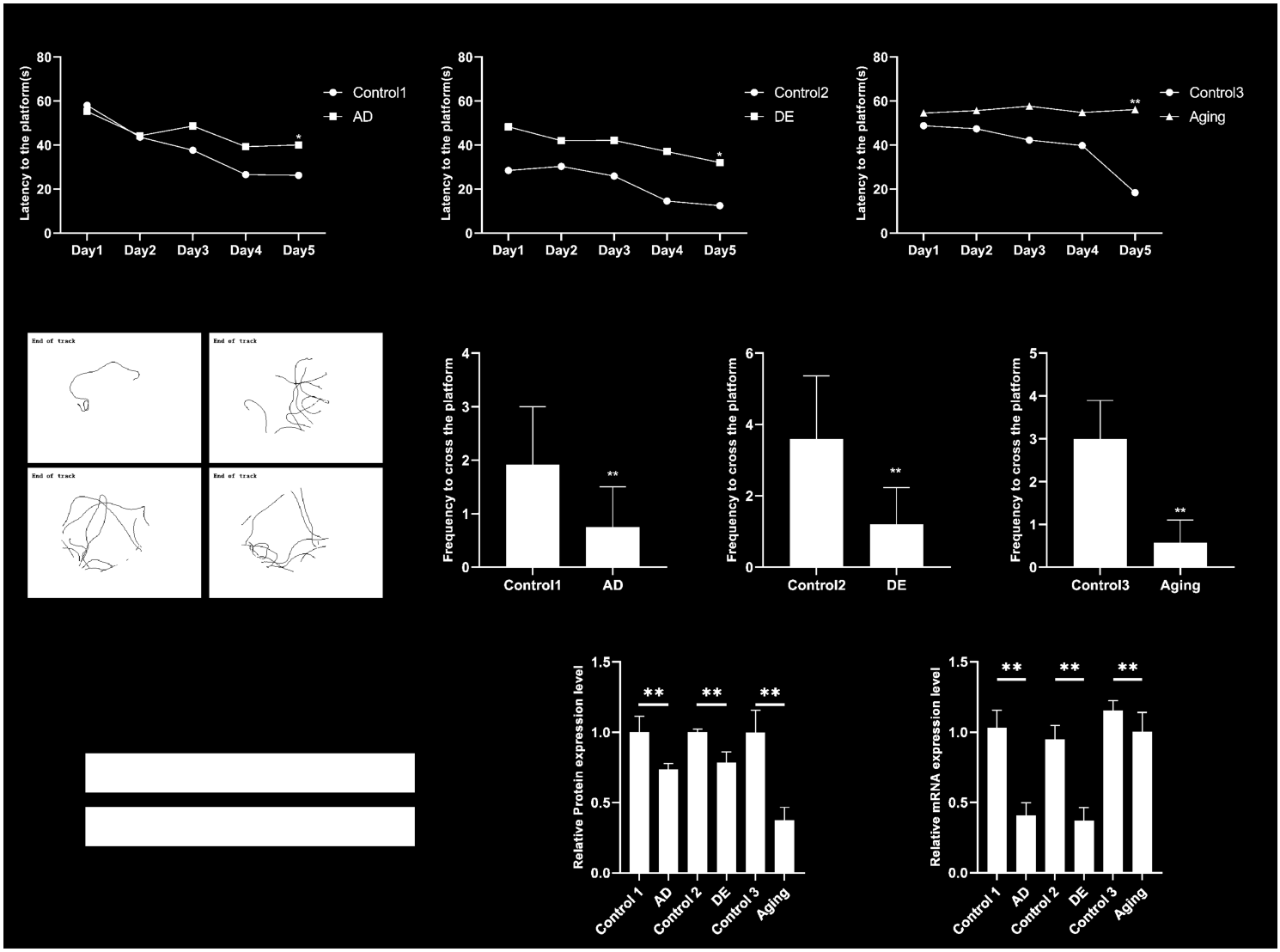

Figure 3

Cognitive impairment is accompanied by reduced hippocampal BAIAP2 expression in mouse models of Alzheimer's disease, diabetic encephalopathy, and brain aging. (A) Escape latency during the 5-day place-navigation phase of the Morris water maze in AD, DE, and aging model mice and their respective controls. (B) Representative swimming trajectories during the spatial probe trial after removal of the hidden platform. (C) Latency to first reach the former platform location during the probe trial, used to assess spatial memory retention. (D) Representative Western blot images of BAIAP2 and β-actin in hippocampal tissues from the three model groups and their corresponding controls. (E) Densitometric quantification of hippocampal BAIAP2 protein expression normalized to β-actin. (F) Relative BAIAP2 mRNA expression in hippocampal tissues determined by RT-qPCR. Data are presented as mean ± SD. Statistical comparisons were performed between each model group and its corresponding control group. *P < 0.05, **P < 0.01.

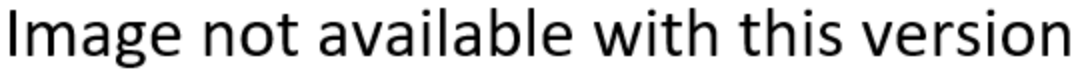

Figure 4

BAIAP2 expression is reduced in the hippocampal CA1, CA3, and dentate gyrus regions of AD, DE, and aging model mice.(A) Representative immunofluorescence images of BAIAP2 in the hippocampal CA1, CA3, and dentate gyrus (DG) regions from control, Alzheimer's disease (AD), diabetic encephalopathy (DE), and aging model mice. BAIAP2 immunoreactivity is shown in green, and nuclei are counterstained with DAPI (blue). Scale bars, 50 μm. (B-D) Quantification of BAIAP2 fluorescence intensity normalized to the analyzed area in the CA1 (B), CA3 (C), and DG (D) regions. BAIAP2 fluorescence was significantly reduced in all three hippocampal subregions in the AD, DE, and aging groups compared with the control group. Data are presented as mean ± SD. **P < 0.01 versus control.

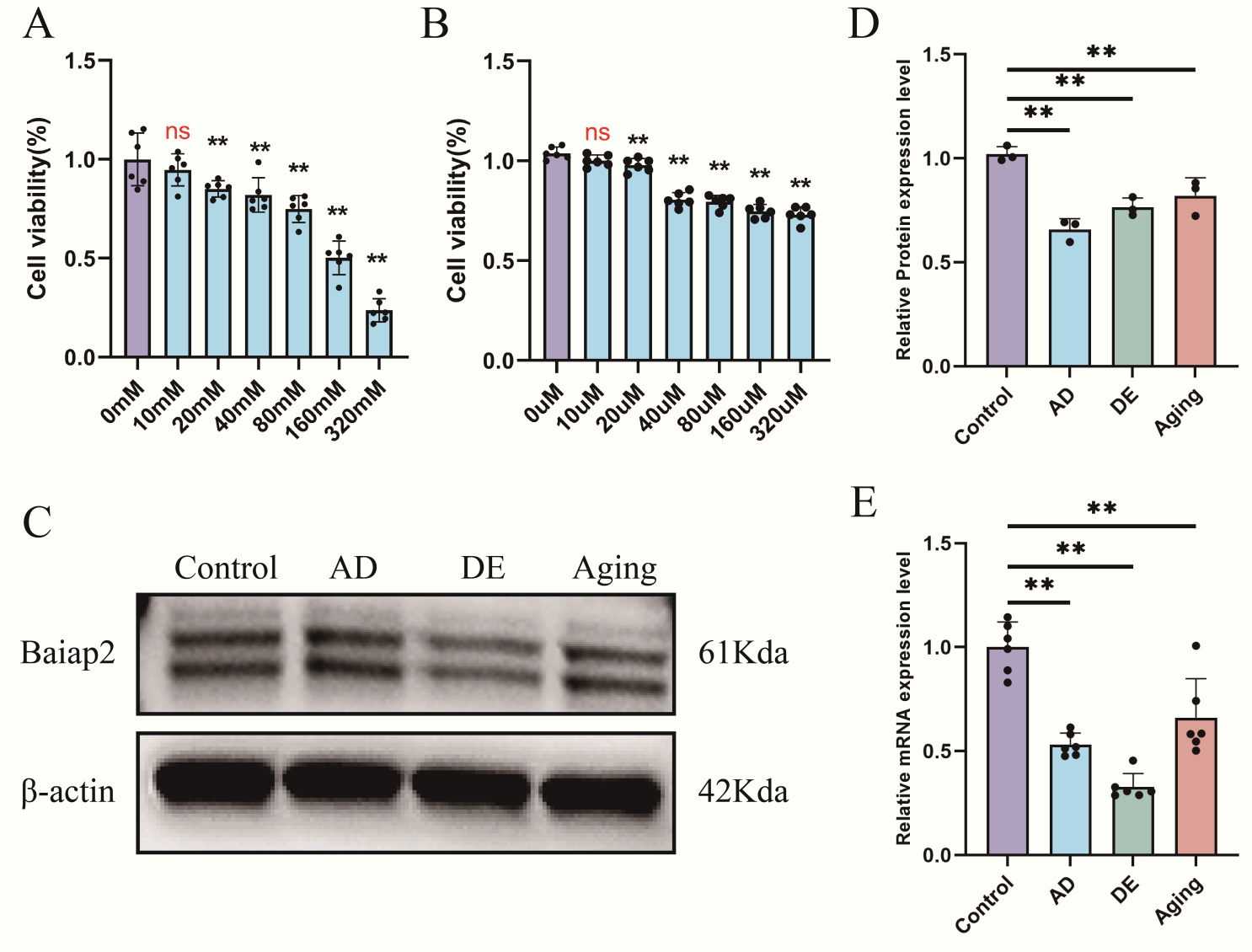

Figure 5

BAIAP2 expression is consistently reduced in SH-SY5Y cell models of AD, DE, and aging-related neuronal stress. (A) CCK-8 assay showing SH-SY5Y cell viability following exposure to increasing concentrations of D-galactose. (B) CCK-8 assay showing SH-SY5Y cell viability following exposure to increasing concentrations of palmitic acid. Cell viability was used to determine treatment concentrations for subsequent experiments. (C) Representative Western blot images of BAIAP2 and β-actin in control cells and in SH-SY5Y cells subjected to AD, DE, and aging-related stress conditions. (D) Densitometric quantification of BAIAP2 protein expression normalized to β-actin. (E) Relative BAIAP2 mRNA expression determined by RT-qPCR. BAIAP2 protein and mRNA levels were significantly reduced under all three pathological stress conditions compared with the control group. Data are presented as mean ± SD. **P < 0.01 versus control.

Supplementary Files

This is a list of supplementary files associated with this preprint. Click to download.

- Graphicabstract.tif